Optical expanders with applications in optical computing

John H. Reif and Akitoshi Yoshida

An optical system called the optical expander is described and investigated. The optical expander electro-optically expands an optical Boolean pattern encoded in d bits into an optical pattern of size N bits. It is assumed that d is equal to $c \log_2 N$ for some constant c, and each expanded pattern is orthogonal to the others. Two different architectures to implement the optical expander are described: one uses an optical matrix–vector multiplier and an array of N threshold devices; the other uses $\log_2 N$ novel reflection–transmission switching cells. These architectures are analyzed in terms of size, energy requirement, and speed. The optical expander described utilizes high-speed and high-space–bandwidth-product connections that are provided by optical beams in three dimensions. Potential applications, holographic memory, and message routing systems are also discussed.

Key words: Optical computing, electro-optical interconnections, holographic memory.

1. Introduction

A. Potential of Optical Computing

Optical computing has recently become an active research field.[1–4] Optics has been used for image processing and long-distance communications as well as for local-area networks. Recently, much attention has been given to the incorporation of optics into very-large-scale-integrated (VLSI) electrical circuits. The possibilities of this approach are contrasted with the limitations of current VLSI technology.[5] VLSI technology is not suitable for interconnection-intensive circuits owing to its two dimensionality, input–output-port (I/O) constraints, and electrical properties such as resistance, capacitance, and inductance. In contrast, optics can utilize free-space interconnects as well as guided-wave technology, neither of which has the above problems. Many researchers have been investigating suitable optical logic devices, interconnection schemes, and architectures. Furthermore, optics may provide drastically new architectures to overcome some architectural problems of conventional electrical computers.[6]

Several theoretical studies have been made to investigate the advantages of free-space optical interconnects.[7,8] The studies indicate that optical interconnects have an advantage over their electrical counterparts in terms of area (volume), speed, and power consumption for high-speed communications, except for the shortest distances within chips.

From the theoretical computational point of view, for a given problem there is a lower bound on the circuit area and its computational time. One such lower bound in the VLSI model, called AT^2 bounds, states that $AT^2 = \Omega(I^2)$, where A is the circuit area, T is the time used by the circuit, and I is the information content of the problem.[9] In a three-dimensional electro-optical model called VLSIO,[10] the similar lower bound can be expressed as $VT^{3/2} = \Omega(I^{3/2})$. This implies that as the information content becomes larger, the VLSI circuit requires a larger and larger area to solve the problem in a fixed amount of time. Using optical interconnection as in the VLSIO model overcomes this interconnection problem by utilizing space in a volume.

In general, replacing electrical devices and interconnects with their optical functional equivalents does not produce good results. We must find a particular area in which optics can be advantageous over electronics. One such area is in holographic memory. Holographic memory may be advantageous over the conventional random-access memory in terms of storage capacity, nonvolatility, and parallel readout capability. Another area is in high-speed dynamic interconnection network systems. Optics is free from various drawbacks found in the two-dimensional (2-D) electrical wiring and thus can provide an interconnection network between a large number of source

The authors are with the Department of Computer Science, Duke University, Durham, North Carolina 27706.

Preprint of paper appearing in *Journal of Applied Optics*, 32, 1993, p. 159-165.

and destination units. However, in spite of this potential, practical implementation has been limited by the lack of an interface that can address or select an element from among a large number of elements by using a small number of control bits.

B. Description of Optical Expanders

The optical expander takes as an input a Boolean pattern of size $d = c \log_2 N$ bits, where c is a constant satisfying $1 \leq c \leq 2$, and expands it to a Boolean pattern of size N bits. Each expanded Boolean pattern must be orthogonal to the others. More precisely, the input to the optical expander is one of N Boolean vectors $p_0, p_1, \ldots, p_{N-1}$, each of length d. We call these vectors the input patterns. Each input pattern is optically encoded by using d pixels, each pixel being ON (denoted by 1) or OFF (denoted by 0). We require each input pattern to have exactly $d/2$ pixels ON, keeping the total power of each pattern equal. From given input pattern p_i, the optical expander produces a spatial output pattern r_i that has exactly one ON pixel at the ith position.

If instead we use an input pattern with more than $d/2$ pixels ON, the output pattern may have several ON pixels. This output can be used for broadcasting messages in an interconnection network or for reading multiple images simultaneously from a holographic memory system.

C. Disadvantage of Conventional Implementation

A line decoder can select an element from among N elements with an input control of $\log_2 N$ bits. A typical VLSI implementation of a large line decoder suffers from two problems. One is due to the topological properties of a VLSI chip. In VLSI, all wires must run on a 2-D plane with a constant number of layers. As N becomes large, even though the logic gates occupy a small area, the interconnections and the I/O occupy a large area, which results in a serious area-utilization problem. The other problem is due to the small fan-in and fan-out of electrical devices. A typical implementation requires a tree structure of logic gates in $\log_2 N$ stages. Furthermore, the I/O constraints may force the chip to transmit N bits in a bit-sequential manner.

Analog beam deflectors based on the acousto-optic effect have several drawbacks. First, they are bulky and require high drive power. Second, they are limited by the capacity–speed product. Our optical expander provides an advantage over these previous approaches by utilizing free space; flexibility and accuracy are provided by digital operations.

D. Outline of Study

In Section 2 we describe applications of our optical expanders. In Section 3 we describe and analyze two different optical expanders: one uses a matrix–vector multiplier and an array of threshold devices, and the other uses $\log_2 N$ identical switches. Finally, Section 4 concludes our study.

2. Applications of Optical Expanders

A. Holographic Memory Storage

Systems that require N distinct entry beams to an N-superimposed hologram may use the optical expander. Holograms can be used to implement random-access memory systems.[11–13] The basic idea of holographic memory storage is to arrange data in blocks and to store them in holograms. A large block of memory can be retrieved at one time simply by illuminating the holograms with the memory's reconstruction beam. This type of memory is particularly suited for read-only applications, since the holograms can be fixed. However, dynamically modifiable holograms such as photorefractive materials may be useful for active holographic memory systems. Research in the 1970's promised the advantages of holographic memory over other types of memory in terms of bit-to-volume ratio, size, and throughput. However, the lack of appropriate recording materials and fast addressing methods kept the progress of holographic memory behind that of conventional bipolar or metal-oxide-semiconductor-based memory. Recently, advances in both recording materials and microlasers have permitted holographic memory to be efficiently implemented.[14,15]

In a typical holographic memory system the data are organized in blocks. N blocks are stored either in a single multiple-exposure volume hologram or in an array of $\sqrt{N} \times \sqrt{N}$ holograms. For either case, N distinct beams are necessary to retrieve N blocks. Our optical expanders can produce these distinct beams from a small number of inputs.

B. Message Routing

Systems that require N distinct entry beams to an array of N devices also may use the optical expander. Message routing is a task in which messages are moved among various processing units. We assume that there are N processors and N messages; each processor has a distinct message with a distinct destination address. Simultaneously, each message is routed from its source processor to its destination processor.

The full advantage of parallelism is realized only if each processing unit has a direct communication path to every other processing unit. In such a case each processing unit can process its data without having serious communication delays, thus resulting in high overall throughput rates. Otherwise, the communication cycle may far exceed the processing cycle, and this will cause a serious bottleneck in the overall system speed.

The highest level of interconnection is a crossbar network that uses N^2 interconnects to connect N source units and N destination units. The number of electrical interconnection wires required by each processing unit to communicate with the other processing units on- and off-board limits the feasible size of the network. To overcome the problem, researchers have proposed optical crossbar networks.[16–18] An $N \times N$ spatial light modulator (SLM) is typically

used to connect N source processors to N destination processors. Each source processor uses a column of the SLM to address one of N destination processors. The advantage of this optical crossbar is that once all the entries of the SLM are set, the message can be transmitted at a high rate. However, there are two drawbacks. First, at most, $1/N$ of the power incident upon the SLM reaches the detector. Second, it takes a long time to electrically set an $N \times N$ SLM.

For faster switching and higher efficiency a network that uses fixed multiple-exposure holograms has been proposed.[19] Unlike the matrix–vector-multiplier-based optical crossbar networks, this holographic interconnection network uses fixed holograms to steer spatially encoded light beams that are transmitted from the source units toward the destination units. In this scheme each address is encoded as a nonorthogonal pattern of size $\sqrt{2N}$ bits. The system cross talk is distributed among different detectors by increasing the dimensionality of the detector plane. To further reduce the cross talk, one must employ N orthogonal patterns to address the holograms. Our optical expanders can create such N orthogonal optical patterns.

3. Optical Expanders

Our first approach uses a matrix–vector multiplication followed by a threshold operation. We call this the matrix–vector mutiplier optical expander. First, we describe two different encoding schemes that can be used in this model. Our second approach is based on a novel idea of using only $\log_2 N$ identical switches to digitally deflect the laser beam. We call this the digital beam deflector (DBD) optical expander.

A. Matrix–Vector Multiplier Optical Expander

1. *Encoding of Input*

The first scheme employs $c = 2$. Each pattern p_i consists of two bit strings: one encodes i in binary and the other is the complement of the first. If this is considered too large, we can set d smaller than this value. To do this, we can recursively enumerate a set of bit strings with $d/2$ 1's and 0's. We show that this gives $c \approx 1$ for large d. We can analyze this encoding by using Stirling's formula $x! \approx \sqrt{2\pi x}x^x \exp(-x)$ to find the asymptotic value of c:

$$c \approx \frac{d}{d + \frac{1}{2}\log_2 \frac{2}{\pi d}}.$$

Thus, for a large d, c approaches 1. This encoding produces a larger N as d increases. For example, $d = 14$ yields $N = 3432$ in this encoding, whereas in the first encoding we have $N = 2^7 = 128$.

2. *Matrix–Vector Multiplication*

The $N \times d$ matrix consists of N rows, in which the ith row represents p_i. Let p_k be an input to the matrix–vector multiplier. Then, the result of the multiplication is an output vector of length N, in which the ith element of the vector is the inner product of p_k and p_i:

$$\begin{bmatrix} p_0 \\ \cdots \\ p_{k'} \\ \cdots \\ p_k \\ \cdots \\ p_{N-1} \end{bmatrix} (p_k)^T = \begin{bmatrix} \cdots \\ \cdots \\ 0 \\ \cdots \\ d/2 \\ \cdots \\ \cdots \end{bmatrix}.$$

Here, $(p_k)^T$ represents the transposed vector of pattern p_k.

The output vector has value $d/2$ (in relative units) at the kth position and has a 0 value at the k'th position, where $p_{k'}$ is the bit-wise complement of p_k. Other elements in the output vector have values between 0 and $d/2$. We apply a threshold operation at a certain intensity level to produce one of the N orthogonal patterns.

3. *Optical Matrix–Vector Multiplier*

Optical matrix–vector multipliers have been proposed and experimentally demonstrated.[4,20] We need to multiply a fixed matrix of size $N \times d$ with an input vector of length d. We can arrange this input vector I, the matrix M, and the output vector $\mathbf{O}$ into nearly square shapes. This means I, M, and $\mathbf{O}$ are formatted in $\sqrt{d} \times \sqrt{d}$, $\sqrt{dN} \times \sqrt{dN}$, and $\sqrt{N} \times \sqrt{N}$ arrays, respectively. The examples are shown in Fig. 1 with $d = 4$ and $N = 6$. The matrix plane is divided into d blocks arranged in a $\sqrt{d} \times \sqrt{d}$ array. The ith column of the matrix is represented by the ith block. Each block has N elements that represent elements of the column.

In operation, when the ith source is ON, it creates a pattern of the ith block through a fixed mask or grating, which is omitted in the figure. At the matrix plane, the product of the ith column of M and

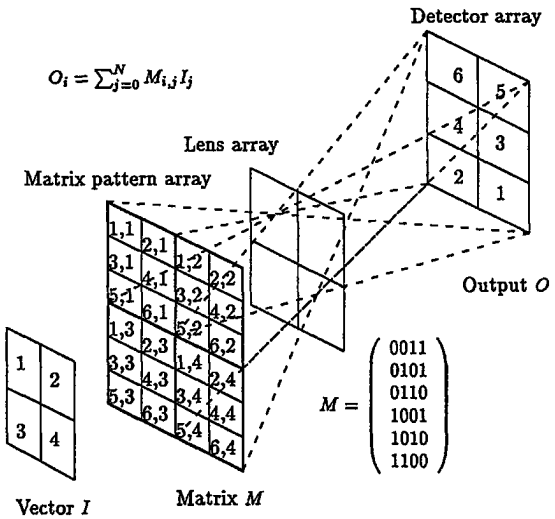

Fig. 1. Matrix–vector multiplication.

the ith element of $\mathbf{I}$ is obtained at the ith block. The light waves from all the blocks are superimposed at the detector array, and thus the product is obtained.

4. Threshold Operation

A nonlinearity must be introduced to generate a set of N orthogonal boolean patterns from a set of N distinct d-linear independent Boolean patterns. As we recall, the output vector from the matrix–vector multiplier has a value $d/2$ at the kth position and has value 0 at the k'th position.

One possibility is to set the threshold value at $d/2$. This method works as long as d is small. However, when d becomes relatively large, it is difficult to distinguish intensity $d/2$ from intensity $d/2 - 1$. Our solution is to distinguish intensity 0 from intensity 1, since the output vector also has exactly one position that has intensity 0. Then, the complement of the output becomes orthogonal. In this approach we need be concerned not with the physical limit of the threshold device but rather the sensitivity and the dynamic range of the device.

5. Overall Architecture and Analysis of Matrix–Vector Multiplier Optical Expander

The overall architecture is shown in Fig. 2. For convenience we assumed $d = \log_2 N$ for this analysis. An array of $\log_2 N$ light sources produces input to the system. We call them the primary sources, since they are active sources. Each primary source produces a block of N secondary sources through mask or a grating. Each block of the secondary sources is imaged upon the detector array by its associated lens. There are $\log_2 N$ blocks, and each block has N secondary sources. There are $\log_2 N$ lenses and N detectors. Let S_s, S_l, and S_d be the transverse dimensions of the secondary source, the lens, and the detector arrays, respectively. The spacings between the secondary sources, the lenses, and the detectors are represented by s_s, s_l, and s_d, respectively. Let l_f, l_b, and L be the distances between the secondary source and the lens arrays, the lens and the detector arrays, and the secondary source and the detector arrays.

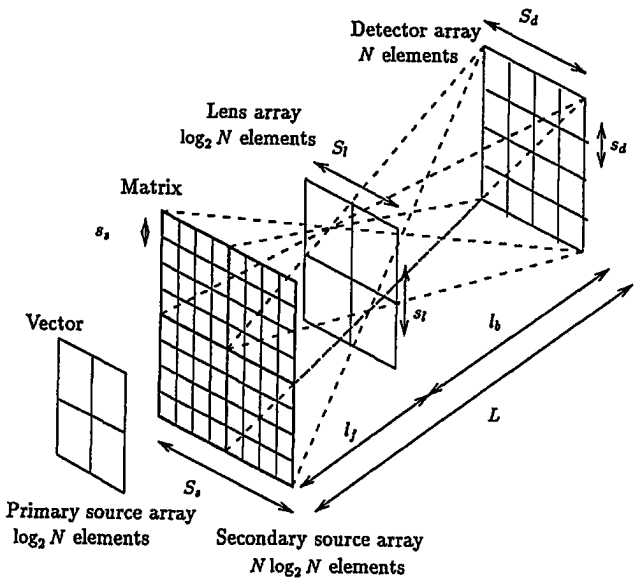

Fig. 2. Matrix–vector multiplier optical expander.

We now analyze three issues concerning the matrix–vector multiplier optical expander. The first issue is due to the aberration of the system. The second concerns the diffraction limit imposed by the system. The third concerns the fan-out factor, which depends on the minimum detectable power of the detectors at a given operating condition. The theoretical limits on the scalability of the system can be analyzed by using several parameters.[21]

Aberration Limit. The spherical aberration and the coma aberration can be eliminated by optimizing the shape of the lenses. The astigmatic aberration becomes dominant for off-axis imaging, since it cannot be eliminated. Let Y_0 be the displacement of the source from the optical axis. The displacement of the image owing to the astigmatic aberration ΔY_1 can be expressed as

$$\Delta Y_1 = \nu(1 + \alpha)\frac{s_l}{l_f^2} Y_0^2,$$

where $\nu = (3n + 1)/4$ depends on the index of refraction n of the lens and $\alpha = l_b/l_f$ represents the lateral magnification.[22]

The relationship between the source spacing and the detector spacing can be written as $s_d = \alpha s_s$. The detector spacing must be set to greater than the displacement caused by the aberration to avoid cross talk from neighbors. Thus $2\Delta Y_1 \le s_d$. We obtain

$$\frac{2Y_0^2\nu(1 + \alpha)^3 s_l}{L^2} \le \alpha s_s.$$

The image of a single block has a transverse dimension $\sqrt{N}\alpha s_s$. The spacing between this image and the one produced by the same block by its adjacent lenses is $(1 + \alpha)s_l$. To avoid overlapping, we must have

$$\sqrt{N}\alpha s_s \le (1 + \alpha)s_l.$$

Combining these two inequalities, we obtain

$$\frac{2Y_0^2\nu\sqrt{N}(1 + \alpha)^2}{L^2} \le 1.$$

The maximum displacement of a source from its optical axis occurs between the source block and its lens at a corner, and it is obtained by

$$Y_0 = \frac{1}{\sqrt{2}}\left(S_s - S_l + \frac{S_l}{\sqrt{\log_2 N}}\right) = \frac{S_l}{\sqrt{2}}\left(\frac{\alpha + \sqrt{\log_2 N}}{\alpha\sqrt{\log_2 N}}\right)$$

Thus we have the following condition:

$$\frac{\beta^2(\alpha + \sqrt{\log_2 N})^2}{\alpha^2 \log_2 N}(1 + \alpha)^2\nu\sqrt{N} \le 1,$$

where $\beta = S_l/L$ represents the normalized lens size.

Figure 3 displays the maximum β for given α and N. For a given N, possible values for α and β lie below its curve.

Diffraction Limit. The finite size of a lens aperture limits the minimum spot size formed by the lens. This spot size must be smaller than the detector spacing to avoid cross talk owing to diffraction. This condition can be written as

$$\frac{2.44 l_b \lambda}{s_l} \leq s_d,$$

where s_l, l_b, and λ are the aperture size, the distance from the lens to the image, and the wavelength, respectively.

Using the same parameters as before, we obtain

$$\frac{2.44\alpha\lambda\sqrt{N}\log N}{(1+\alpha)^2\beta^2 L} \leq 1.$$

Figures 4 and 5 show the minimum β for given α and N for $L = 0.01$ m and $L = 0.1$ m, respectively. In these figures the region above each curve represents possible values for α and β. As N increases, L must increase so that possible values for α and β exist within the aberration and diffraction limits.

Power Limit. Finally, we consider the power limit. We ignore some constant factor losses in the system. A strong practical limit on the maximum N is not determined by the above analysis on aberration and diffraction, but by a simple analysis on the power distribution limit. Let P_0 be the radiation power from a single primary source. We assume that this power is distributed to N secondary sources with efficiency η, and each secondary source has the radiation angle θ. The power received at a detector is

$$P_r = \frac{\eta P_0 s_l^2}{2\pi N l_f^2 (1 - \cos\theta)}.$$

Using the same parameters as before, we obtain

$$P_r = \frac{\eta P_0 \beta^2 (1+\alpha)^2}{2\pi N \log_2 N (1 - \cos\theta)}.$$

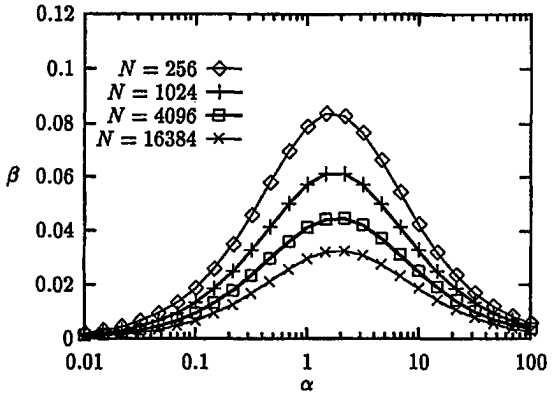

Fig. 3. Maximum N determined by aberration. The region below each curve represents possible values of α and β.

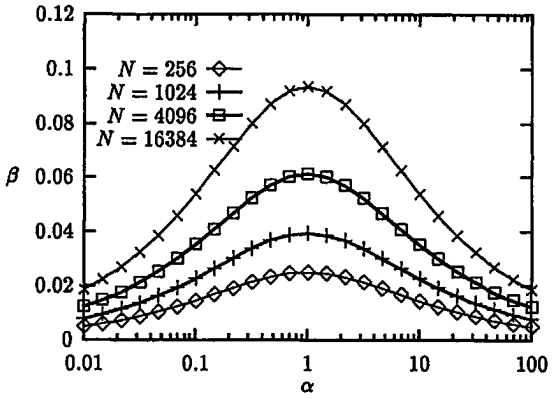

Fig. 4. Maximum N determined by diffraction at $L = 0.01$ m. The region above each curve represents possible values of α and β.

The minimum detectable power depends on the required bit error rate and the bit rate. We assume that the bit error rate is 10^{-17}, the primary source power $P_0 = 2$ mW, the efficiency $\eta = 0.5$, and the radiation angle $\theta = 5°$. Using data from Ref. 23, we assume that the minimum detectable power is -57 dBm at 1 Mbit/s and -30 dBm at 1 Gbit/s. We calculate the maximum N for a given bit rate in Fig. 6. For a bit rate of 100 Mbits/s, N can be in the hundreds. For larger N, more sensitive detectors or slower bit rates must be used.

B. Digital Beam Deflector Optical Expander

In this architecture we use $\log_2 N$ switching cells to deflect an input laser beam. Once the switches are set, data can be transmitted by a pulse-modulated optical beam at an extremely high rate. A multiple-stage digital laser beam deflector was previously developed,[24] but it had several disadvantages such as a high drive voltage and a large switch size. Another approach may be to use a tree structure of N switching cells in $\log_2 N$ stages. Each switch can be a conventional electro-optic directional coupler.[25] The construction of an optical expander with this approach requires a total of N switches configured in a complete binary tree structure of depth $\log_2 N$. The switch size is kept small for each node. However, it requires N switches.

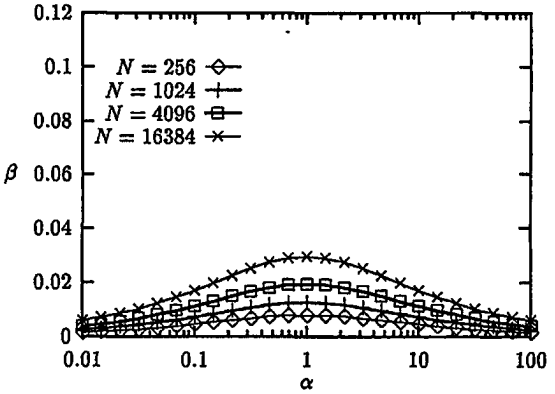

Fig. 5. Same as Fig. 4 but with $L = 0.1$ m.

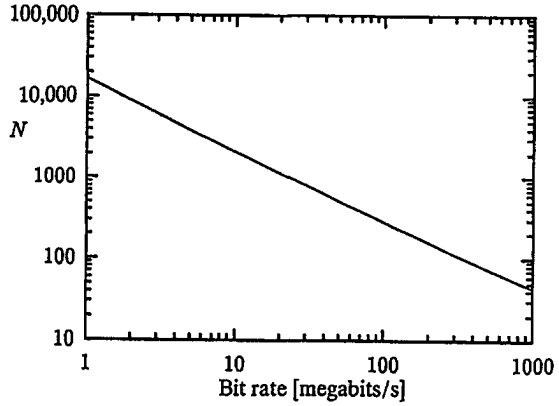

Fig. 6. Maximum N determined by power distribution.

Our approach does not suffer the drawbacks of these previously proposed systems. It uses only $\log_2 N$ small switches.

We designed a reflection–transmission cell and a deflector as shown in Figs. 7 and 8. The switches have reflection and transmission states. Throughout the stages, the range of the incident angles is kept constant by keeping the ratio of the aperture size to the focal length constant. The minimum switch size associated with each stage increases as the focal length increases. Assuming that the beamwidth is significantly larger than the wavelength, we see that the switch size can be kept much smaller than the aperture size. At the final stage, the output beam must exit at an appropriate location.

At each stage the laser beam hits the cell at a certain angle within a fixed range. The beam is reflected or transmitted at each switch, depending on the control signal. Figure 8 shows all possible paths of the beam. At the ith stage there are 2^{i-1} distinct incident angles within the range. Currently, our choice in realizing a reflection–transmission cell is limited; nevertheless, several approaches are considered below.

One possibility is to use an optical switch based on electrochemically generated bubbles.[26] The switching element is a slot filled with a fluid. If there is no bubble in the slot, the incident light is transmitted. When a bubble is electrochemically introduced to the slot, the incident light experiences a total internal reflection from the slot. This is a novel bistable optical switch that is both polarization and wavelength independent. However, the switching speed is too slow for rapidly switching networks. On the other hand, if the network is static for a time of the order of minutes and does not require fast switching, this may provide an efficient data transfer at a high

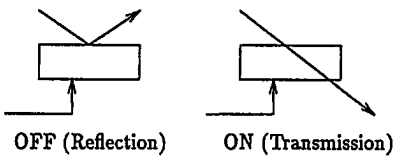

Fig. 7. Reflection–transmission cell.

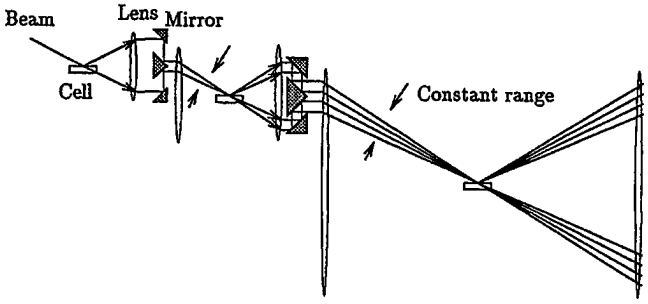

Fig. 8. DBD optical expander.

bit rate. For such applications, one may use mechanically controlled mirrors.

Another possibility is to use polarization-dependent materials such as a nematic-liquid-crystal switch.[27] The switching speed is limited by that of the nematic liquid crystal. To achieve a higher switching speed, we could use an alternative approach of keeping the nematic-liquid-crystal switch as a static polarizing beam splitter and using a much faster ferroelectric liquid-crystal polarization rotator.[28,29]

It is possible that an alternative material will be discovered. Then, a significantly simpler and more efficient beam deflector could be constructed.

C. Overall Architecture and Analysis of Digital Beam Deflector Optical Expander

In this model the control signal encoded in $\log_2 N$ bits controls the $\log_2 N$ stages of the cells. The total length of the system is proportional to N. If the switches are ideal, it is easy to construct a 2-D version of the DBD optical expander, shown in Fig. 9. The maximum N is determined by insertion loss and cross talk.

A false reflection and transmission introduces loss and cross talk. The insertion loss and the cross talk depend on the switching devices. Thus we avoid a particular analysis here.

We assume that each switch has a correct reflection-and-transmission rate μ and a false rate $1 - \mu$, and we ignore other factors. The total loss becomes $1 - \mu^{\log_2 N}$. The cross talk does not accumulate through the stages and is bounded above by $(1 - \mu)/\mu$.

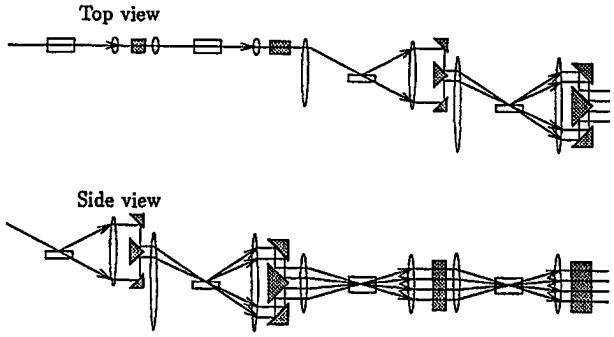

Fig. 9. 2-D version of DBD optical expander.

4. Conclusion

We have investigated a problem of electro-optically creating one of the N mutually orthogonal Boolean patterns from a given input pattern encoded in $c \log_2 N$ bits, where c is a constant no greater than 2. Two approaches were considered and investigated: one was based on optical matrix–vector multiplication followed by a threshold operation; the other was based on a digital beam deflector. We also discussed applications of optical expanders and showed the importance of the design and the development of our optical expanders.

The authors thank Robert Guenther for useful discussions and the anonymous reviewers for their valuable comments. This research was supported in part by U.S. Air Force Office of Scientific Research contract AFOSR-87-0386, U.S. Office of Naval Research contract N00014-87-K0310, and Defense Advanced Research Projects Agency/Army Research Office contract DAAL03-88-K-0195.

References

1. A. A. Sawchuk and T. C. Strand, "Digital–optical computing," Proc. IEEE **72,** 758–779 (1984).
2. T. E. Bell, "Optical computing: a field in flux," IEEE Spectrum **23**(8), 34–57 (1986).
3. D. Feitelson, *Optical Computing, A Survey for Computer Scientists* (MIT, Cambridge, Mass., 1988).
4. H. J. Caulfield, J. A. Neff, and W. T. Rhodes, "Optical computing: the coming revolution in optical signal processing," Laser Focus **19**(11), 100–109 (1983).
5. J. W. Goodman, F. J. Leonberger, S. Kung, and R. A. Athale, "Optical interconnections for VLSI systems," Proc. IEEE **72,** 850–866 (1984).
6. A. Huang, "Architectural considerations involved in the design of an optical–digital computer," Proc. IEEE **72,** 780–786 (1984).
7. D. A. B. Miller, "Optics for low-energy communication inside digital processors: quantum detectors, sources, and modulators as efficient impedance converters," Opt. Lett. **14,** 146–148 (1988).
8. M. R. Feldman, S. C. Esener, C. C. Guest, and S. H. Lee, "Comparison between optical and electrical interconnects based on power and speed considerations," Appl. Opt. **27,** 1742–1751 (1988).
9. J. D. Ullman, *Computational Aspects of VLSI* (Computer Science, Rockville, Md., 1984).
10. R. Barakat and J. Reif, "Lower bounds on the computational efficiency of optical computing systems," Appl. Opt. **26,** 1015–1018 (1987).
11. H. Kiemle, "Considerations on holographic memories in the gigabyte region," Appl. Opt. **13,** 803–807 (1974).
12. L. d'Auria, J. P. Huignard, C. Slezak, and E. Spits, "Experimental holographic read–write memory using 3-D storage," Appl. Opt. **13,** 808–818 (1974).
13. D. Chen and J. D. Zook, "An overview of optical data storage technology," Proc. IEEE **63,** 1207–1230 (1975).
14. S. Redfield and L. Hasselink, "Enhanced nondestructive holograhic readout in strontium barium niobate," Opt. Lett. **13,** 880–882 (1988).
15. E. H. Paek, J. R. Wullert II, M. Jain, A. Von Lehmen, A. Scherer, J. Harbison, L. R. Florenz, H. J. Yoo, J. L. Jewell, and Y. H. Lee, "Compact and ultrafast holographic memory using a surface-emitting microlaser diode array," Opt. Lett. **15,** 341–343 (1990).
16. A. D. McAulay, "Optical crossbar interconnected digital signal processor with basic algorithms," Opt. Eng. **25,** 82–90 (1986).
17. A. A. Sawchuk, B. J. Jenkins, C. S. Raghavendra, and A. Varma, "Optical matrix–vector implementation of crossbar interconnection networks," in *Proceedings of the International Conference on Parallel Processing,* K. Hwang, S. M. Jacobs, and E. E. Swartzlander, eds. (Institute of Electrical and Electronics Engineers, New York, 1986), pp. 401–404.
18. A. A. Sawchuk, B. J. Jenkins, C. S. Raghavendra, and A. Varma, "Optical crossbar networks," Computer **20**(6), 50–60 (1987).
19. E. S. Maniloff, K. M. Johnson, and J. H. Reif, "Holographic routing network for parallel processing machines," in *Holographic Optics II, Principles and Applications,* G. M. Morris, ed., Proc. Soc. Photo-Opt. Instrum. Eng. **1136,** 283–289 (1989).
20. E. P. Mosca, R. D. Griffin, F. P. Pursel, and J. N. Lee, "Acousto-optical matrix–vector product processor: implementation issue," Appl. Opt. **28,** 3843–3851 (1989).
21. T. Sakano, K. Noguchi, and T. Matsumoto, "Optical limits for spatial interconnection networks using 2-D optical array devices," Appl. Opt. **29,** 1094–1100 (1990).
22. M. Born and E. Wolf, *Principles of Optics,* 6th ed. (Pergamon, Oxford, 1980).
23. D. H. Hartman, "Digital high speed interconnects: a study of the optical alternative," Opt. Eng. **25,** 1086–1102 (1986).
24. H. Meyer, D. Riekmann, K. P. Schmidt, U. J. Schmidt, M. Rahlff, E. Schröder, and W. Thust, "Design and performance of a 20-stage digital light beam deflector," Appl. Opt. **11,** 1732–1736 (1972).
25. K. Iizuka, *Engineering Optics,* 2nd ed. (Springer-Verlag, New York, 1987).
26. J. L. Jackel, J. J. Johnson, and W. J. Tomlinson, "Bistable switching using electrochemically generated bubbles," Opt. Lett. **15,** 1470–1472 (1990).
27. R. A. Soref and D. H. McMahon, "Total switching of unpolarized fiber light with a four-port electro-optic liquid-crystal device," Opt. Lett. **5,** 147–149 (1980).
28. L. R. McAdams, R. N. McRuer, and J. W. Goodman, "Liquid-crystal optical routing switch," Appl. Opt. **29,** 1304–1307 (1990).
29. L. R. McAdams and J. W. Goodman, "Liquid crystal $1 \times N$ optical switch," Opt. Lett. **15,** 1150–1152 (1990).

High-resolution inset head-mounted display

Jannick P. Rolland, Akitoshi Yoshida, Larry D. Davis, and John H. Reif

A novel approach to inset superimposition in a high-resolution head-mounted display (HMD) is presented. The approach is innovative in its use of optoelectronic, nonmechanical devices in place of scanning mechanical devices commonly adopted previously. A paraxial layout of the overall HMD system is presented, and the benefit of employing hybrid refractive-diffractive optics for the optical component that generates the inset is discussed. A potential overall HMD design is finally presented to show the integrated system. The practical limitations of the designed system are discussed and an alternative approach is presented to compare the advantages and the limitations of these systems.

OCIS codes: 090.2820, 220.0220, 050.1380, 230.0250.

1. Introduction

The field of virtual environments (VE's) and the use of head-mounted displays (HMD's) as three-dimensional (3D) visualization devices have recently received considerable attention due to the potential to create unique capabilities for advanced human–computer interaction.[1–3] Such advanced interaction can include interactive control and diagnostic, educational and training, teleoperation, and entertainment systems.[4–9]

Conventional HMD's typically do not utilize the full potential of VE technology. In particular, they are often limited in field of view and resolution, which is critical to the development of various VE applications. Using a small high-resolution inset and a large low-resolution background image can minimize the trade-off of field of view against an effective resolution.[10] The gaze point of the user, which is determined from eye tracking, controls the position of the inset dynamically and thus high effective resolution over a large field is provided. The main advantages of such a dual-display approach are the relatively low-cost displays as a substitution for expensive high-resolution displays, and the reduction in computation and bandwidth needed to update the scenes. Although the user can observe dynamic scenery over a large field at apparent high resolution, the image updates do not have to occur simultaneously at high resolution: the portion of the image near the gaze point may be updated quickly at high resolution; other portions of the image may be updated less frequently or at lower resolution to reduce both the computational load and the transmission bandwidth.

To match human visual acuity within the inset, the inset pixel size must subtend approximately 1 arc min at the eye.[11] From the knowledge that the human retina does not provide uniform visual acuity across its field of view, the resolution of the HMD needs to reach 1 arc min only inside the inset and can be lower over the entire background.[12,13] De facto, human visual acuity degrades significantly as the distance from the fovea increases; at an angular distance of 5° from the center of the fovea, it is approximately a quarter of the highest acuity, and at an angular distance of 15°, it becomes only one seventh of the highest acuity.[11]

Another common shortcoming of conventional HMD's is their lack of integrated effective interaction capabilities combining head and eye tracking. In fact, the interaction capability is ordinarily limited to the use of head tracking to measure the position and the orientation of the user's head and to generate scenery from the user's perspective.[14] This capability allows the user to navigate through the virtual world and interact with the virtual objects with essentially 3D manual input devices. However, for sit-

J. P. Rolland and L. D. Davis are with the Center for Research and Education in Optics and Lasers, Department of Electrical and Computer Engineering, University of Central Florida, 4000 Central Florida Boulevard, Orlando, Florida 32816-2700. A. Yoshida is with the Computing Center at the University of Mannheim, D-68131 Mannheim, Germany. J. H. Reif is with the Department of Computer Science, Duke University, Durham, North Carolina 27708.

Preprint of paper appearing in *Applied Optics: Optical Technology and Biomedical Optics*, 37(19), 4183–4193 (1998).

uations that require response times less than 300 ms or difficult coordination skills, interaction capability supported by such manual input devices becomes inadequate. For those cases, eye movement could be used in conjunction with manual input devices to provide effective interaction methods. Various interaction methods can thus be realized through the use of hand, body, and eye movements.[15–17] Since the eyes respond to stimulus 144 ms faster than the hand,[18–20] they can be used for fast and effective input, selection, and control methods.

An additional advantage of using eye tracking is that image rendering can take advantage of the physiological limitation of the eyes. It has been well known since Reymond Dodge[21] in the 1900's that when the eyes move, information processing is suppressed. This is known, in the modern literature, as saccadic suppression.[22,23] Therefore, although the gaze point is in rapid motion, the image update does not have to occur at full resolution and the fine detail of the scene can be rendered when the gaze point is basically fixed. With eye tracking, image rendering can be carried out according to both head and eye movement. Thus the use of eye tracking is not limited to finding the gaze point for positioning the inset, it can also play a fundamental role in providing another unique means of interaction in the VE. Combined with appropriate computer software, a HMD with eye-tracking capability will become an active vision HMD that gives the user the feeling of being immersed in the virtual environment and provides effective gaze-point-oriented interaction methods.

A common approach to producing a high-resolution inset is to employ large high-resolution displays, or light valves, and transport the high-resolution images to the eyes by imaging optics coupled to a bundle of optical fibers.[24,25] In such an approach, scanning optics that employ, for example, mirrors as the scanning mechanism are used to position the inset at the user's point of gaze. Another more recent approach to a high-resolution inset uses only one light valve and renders the image at the gaze point more accurately than the surrounding image. Although systems employing either approach provide significant improvements over ordinary displays in terms of image quality, they are seldom put to use because they are heavy, expensive, and most important, nonportable.

We propose a radically different approach to the positioning of a high-resolution inset that is illustrated in Fig. 1.[26,27] The approach allows the positioning of the inset without any mechanically moving parts. Instead, the inset is positioned optically with a lenslet array subsystem referred to as the duplicator and shown in Fig. 1. We predict that the use of fixed optoelectronic components allows the whole system to be fabricated with fewer alignment errors, to be immune to mechanical failure, to be more tolerant to vibrations, and to be portable, which is important. Such an approach leads to an optoelectronic high-resolution inset (OHRI) HMD.

In this paper, the optical insertion and superimposition schemes are first presented. The paraxial layout of the OHRI HMD is then given followed by a discussion of the potential use of binary optics for the duplicator. Next, a design configuration for the overall HMD is shown, its performance is demonstrated, and the integration of a low-cost eye-tracker system is presented. Finally, practical limitations of the system are discussed and alternative approaches to the design are presented to access the advantages and the limitations of the proposed system better.

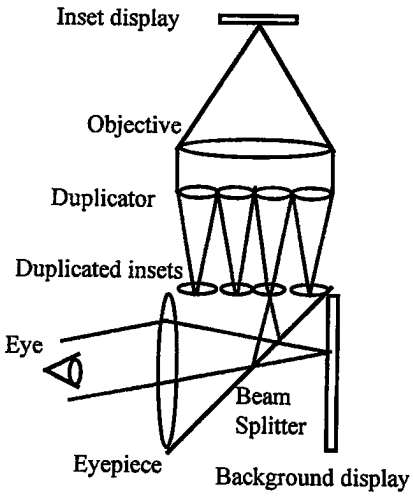

Fig. 1. Schematic diagram of the OHRI HMD.

2. Optical Insertion of the High-Resolution Inset

The basic concept of the OHRI HMD, which is illustrated in Figs. 1 and 2(a), is optical duplication of the inset image into a fixed array of nonoverlapping copies and selection of one copy by blocking the others. The selected copy of the inset image is then superimposed optically on the background image. When the original inset image is partitioned and permuted, as explained in Section 3, it can be positioned at arbitrary locations within the background image. The inset image traces the gaze point, thus the foveated part of the image is seen at high resolution.

The gaze point is determined with eye-tracking

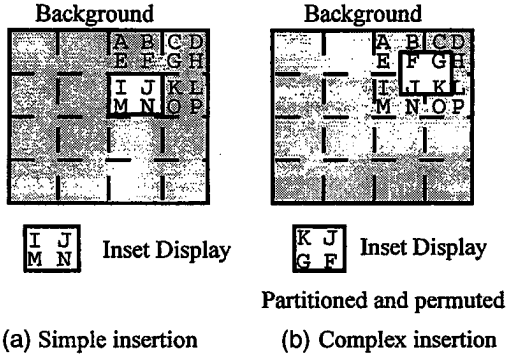

Fig. 2. Superimposition of the inset display: (a) simple insertion and (b) complex insertion with subinset resolution.

technology. Several methods that may differ in accuracy can be used to track eye movements and consequently the gaze points. High-quality head-mounted eye trackers typically produce an accuracy of 1° visual angle.[28,29] For determining the gaze point for the sole purpose of superimposing the high-resolution inset on the background image, the required accuracy can be somewhat lower. For an inset subtending 10°, an accuracy of a few degrees will be sufficient to keep the fovea within the inset. To implement some of the complex human–computer interaction methods with the gaze point, the required accuracy of the eye tracker should essentially match that of the highest-quality commercial eye trackers. Once the gaze point is determined, the superposition of the high-resolution inset over the low-resolution background is carried out with fixed optical components as the imaging devices and liquid-crystal technology as the selection devices. The eye-tracker system proposed for the OHRI HMD is described in Section 8.

Figure 1 shows that two displays are required: one for the background and the other for the inset. The image of the inset display is duplicated optically to fill the entire background display, and a liquid-crystal device array located close to the duplicated images is used to select one element of the array. Only one copy of the inset display image passes through the liquid-crystal array, and all the other copies are blocked. The images of the inset display and the background display are then combined with a beam splitter. The inset may be simply superimposed on the background without blocking its low-resolution counterpart image behind the inset. In this case, the inset portion of the image becomes brighter than the peripheral image. The background image behind the inset may be dimmed electronically to control the effective brightness of the inset. To minimize the boundary effect at the periphery of the inset, one can soften the boundary of the inset either electronically at the inset display or optically with an optical filter inserted in the inset path. An alternative is to use another liquid-crystal device in front of the background display to block the low-resolution counterpart of the inset location. In this case, boundary effects can then be handled in a similar way.

The imaging sequence of the inset path can be described more precisely as follows: emitted light from the inset display is collimated by an objective lens. A first lenslet array then divides and focuses the collimated light to a set of identical images or duplicates of the inset display. This lenslet array constitutes the first layer of the duplicator. The chief rays from the duplicate image points are then set parallel (i.e., telecentric configuration) to the optical axis by another lenslet array that constitutes the second layer of the duplicator. This telecentric arrangement constrains the chief rays in eye space to converge to the location of the entrance pupil of the eye as described in Section 4 and illustrated in Fig. 3. An array of liquid-crystal shutters placed at the duplicator passes one of the duplicated images and blocks the other images. Shutters with switching speeds of as much as 250 Hz are technically possible.[30] The duplicated images are located with respect to the optics so that they are the optical conjugates of the background display (i.e., they are located symmetrically to the background display with respect to the beam splitter). The eye can then see the combined inset-background image through the eyepiece. Although Fig. 1 is a schematic of the objective with a single lens, the duplicator with two lenslet arrays, and the eyepiece with another single lens, each subsystem (i.e., the objective, the duplicator, and the eyepiece) is implemented with multiple optical elements. A possible design configuration for the overall system is given thereafter.

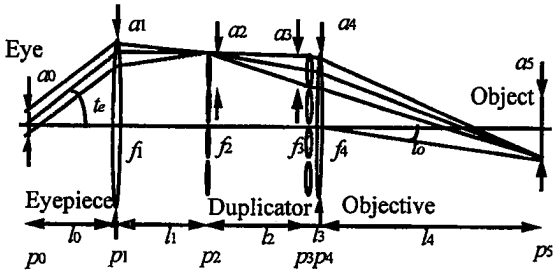

Fig. 3. Paraxial layout of the inset optical path, unfolded with respect to the beam splitter.

3. Simple and Complex Insertion Schemes

The superimposition of the inset and the background is depicted in Figs. 2(a) and 2(b) by a simple and a more complex insertion scheme, respectively. In both figures the shaded areas correspond to the background and the bright areas correspond to the inset. The character symbols represent contents of the image, and the dashed lines represent the cell boundary of the duplicated images.

For a simple insertion scheme, the insertion may be made at discrete nonoverlapping cell locations. In this case, the liquid-crystal array, which may be placed anywhere inside the duplicator, blocks all the duplicated images except for one copy. When the inset image of I J M N is desired at a particular cell location, as shown in Figure 2(b), this image can be directly displayed from the inset display. The duplicated images of I J M N fill every cell, and the copy of this image at that cell location exits the duplicator to be superimposed on the background.

Interestingly, the system is not limited to discrete nonoverlapping inset locations. A complex insertion scheme can be used instead so that the insertion may be made at continuous locations, up to the pixel resolution of the liquid-crystal array. In this case, the size of the inset must be smaller or equal to the size of a single duplicated image. The liquid-crystal array, which must be now placed near the duplicated image plane, blocks all the duplicated images except for some portions of as many as four copies. When the inset image of F G J K is desired at a particular

location, as shown in Fig. 2(b), this image may be partitioned and permuted to K J G F, and the transformed image can be displayed from the inset display. The duplicated images of K J G F fill every cell, and the portions of the four adjacent copies at that location, which form the image of F G J K, exit the duplicator to be superimposed on the background.

Depending on the required resolution of the inset imposed by the VE application, either of the two schemes described here can be adopted. In the case of the complex insertion, the required permutation can be implemented in hardware. A special purpose chip would be required, and the speed of superimposition update could be optimized. Such a chip can be designed by Evans and Sutherland.[31]

4. Paraxial Layout of the Overall Optical System

The overall optical system is folded into two optical paths: one path is dedicated to the generation of the inset and the other allows the generation of the low-resolution background. The two optical paths are combined through a beam splitter before reaching the eyes of the user. Figure 3 shows the basic configuration of the optoelectronic system employed for duplicating the inset image, unfolded with respect to the beam splitter. In this figure the rightmost element is the inset display and the leftmost element is the eye. A thin-lens paraxial model of this system is first derived. In this paraxial model, p_i, with $i = 1 \ldots 5$, represents planes along the optical system (Fig. 3). More specifically, the eye pupil resides at p_0 and the display object resides at p_5. Going from right to left on the figure, the first component is the objective lens, located at p_4, which collimates the light from the display. The lens of the objective has a focal length f_4.

The second component is a two-layer array of telecentric lenses located at p_3 and p_2. We call this double-layer array of lenses the duplicator. The two lenslet arrays have focal lengths f_3 and f_2. The first layer at p_3 duplicates the display image from the collimated light and forms an intermediary duplicated image of the object at p_2, as also shown in Fig. 4(a). The second lenslet array, which aligns the principal rays parallel to the optical axis, as shown in both Figs. 3 and 4(a), is a catalyst for the chief rays to all pass through the center of the eye pupil. This array, however, introduces not only an additional alignment challenge but also a possible visual quality problem because it must be placed at or very close to the intermediate image plane and any scratches or dust on its surfaces significantly degrade the image quality. Furthermore, the lens boundaries may introduce an annoying blocking effect. An alternative to positioning the lens at the location of the intermediary image plane (i.e., plane p_2) is to defocus that lens slightly. Another alternative is to remove the lens, as shown in Figure 4(b). In this case, however, the bundle of rays suffers 50% vignetting at the edges.

The third component, which is located at p_1, is the eyepiece. In the configuration shown in Fig. 3, the

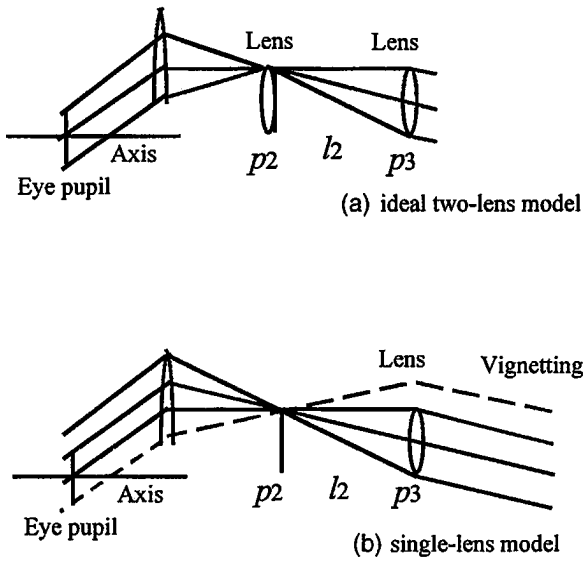

Fig. 4. (a) Ideal two-lens duplicator and (b) single-lens duplicator with vignetting.

intermediary images are located in the focal plane of the eyepiece lens, therefore, they are collimated in eye space. Collimation is not required, as long as the final images are within the range of accommodation of the user, which is typically from 250 mm to infinity. The eyepiece uses a lens with focal length f_1, and the eye is placed at p_0.

Let us denote the distance between planes p_i and p_{i+1} and the diameter of the aperture at p_i, l_i and a_i, respectively; the number of duplicated images along the vertical or the horizontal axes, k; the largest chief-ray angle at the eye pupil, t_e; and the largest angle of the inset object subtended at the apex of the objective lens, t_o. These parameters play essential roles in the paraxial model layout. The basic imaging condition just described and modeled in Fig. 3 yields the following paraxial relationships among the design parameters:

$$f_1 = l_o = l_1, \tag{1}$$

$$l_0 \tan t_e = k a_2/2, \tag{2}$$

$$f_2 = f_3 = l_2, \tag{3}$$

$$l_2 \tan t_o = a_2/2, \tag{4}$$

$$f_4 = l_4, \tag{5}$$

$$l_4 \tan t_o = a_5/2, \tag{6}$$

$$a_0/a_3 = l_1/l_2, \tag{7}$$

$$a_3 = a_2, \tag{8}$$

An implementation of this paraxial layout is presented.

5. Paraxial Design Implementation

This specific implementation assumes two active-matrix liquid-crystal displays from Kopin[32]: a 0.75-

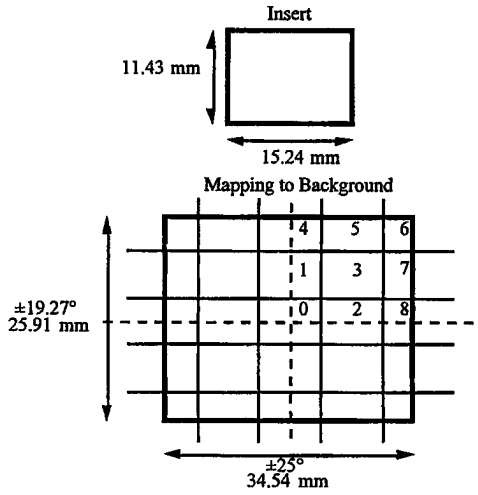

Fig. 5. Mapping of the inset on the background.

in. (1 in. = 2.54 cm) inset display and a 1.7-in. background display. Both displays have 640 × 480 gray-scale pixels. The contrast ratio of the display is 80:1 and each pixel can be addressed in 49 ns, yielding a frame rate of 72 frames/s. We discuss in Section 8 how this frame rate relates to requirements on eye-tracking technology. The system was optimized for 547 nm (±5 nm). A color filter is used to produce monochromatic images from the displays. The typical spectral width is 10 nm for such a filter (e.g., standard bandpass filters form Coherent Ealing). The inset image is magnified (magnification is naturally <1) into one sixteenth of the background image, as shown in Fig. 5. The size of the inset display is 15.24 × 11.43 mm^2, and the size of the background display is 34.54 × 25.91 mm^2. The area of the background display is partitioned into 25 nonoverlapping cells. The inset display is mapped optically into one of these cells for superimposition. There are 3 × 3 full-inset cells, 12 half-inset cells at both the horizontal and the vertical edges, and 4 quarter-inset cells at the corners. The cells at the upper right quadrant are numbered from 0 to 8. The other quadrants are symmetrical to this quadrant, and the performance at one quadrant is fully representative of the entire system. We investigated the upper right quadrant.

The following parameter values were selected according to available display devices and design tradeoffs, and they are summarized in Table 1. We selected a_0, the diameter of the eye pupil, to be 10 mm; a_5, the diameter of the high-resolution display, to be 15.24 mm; ka_2, the diameter of the array of duplicated images, to be 34.54 mm; t_e, the maximum chief ray angle at the eyepoint, to be 25°; and k, the number of duplicated images along the duplicated array diameter, to be 4. From these values and Eqs. 1–8, the maximum half-field angle of the objective lens, t_o, is 7.69°. All parameter values a_i, f_i, and l_i are determined and are listed in Table 2. These parameters are used to design each component of the high-resolution inset system (i.e., the objective lens, the duplicator, and the eyepiece). As smaller displays become available on the market, smaller and more compact systems may be built. In fact, Kopin has recently manufactured a 0.24-in. display with 320 × 240 pixels that may be used with their 0.75-in. display to build such a compact system.

Table 2. Design Value Parameters (mm)

i	a_i	f_i	l_i
0	10.000	—	37.036
1	—	37.036	37.036
2	8.635	31.980	31.980
3	8.635	31.980	—
4	—	56.442	56.442
5	15.240	—	—

[a]Given in millimeters.

6. Design of the Duplicator with Binary Optics

The duplicator arrays can employ either conventional or binary optics technology. The disadvantage of using conventional optics for the duplicator lenslet arrays is the high sensitivity to misalignment. An alternative is to use binary optics where the lenslet array is fabricated on one substrate. This approach solves the problem of aligning the individual lenses in the arrays. A fill factor of 100% is assumed for the binary optics array because spacing of less than 10 μm can be achieved in binary optics arrays fabrication. The minimum feature size determined by the fabrication facility limits the smallest f-number of the lens to be fabricated. For analytic binarization, the minimum feature size occurs at the edges of the lens.[33] Starting with the grating equation, the definition of the f-number, and the assumption that the feature size is small compared with the lens diameter and the focal length, gives as the minimum feature size of p

$$p = \frac{\lambda}{m}\sqrt{1 + 4(f_\#)^2}, \tag{9}$$

where λ is the wavelength, m the number of phase levels, and $f_\#$ the f-number of the lens.

Table 1. Basic Design Parameters

Parameters	Background	Inset
Display size	34.54 mm × 25.91 mm	15.24 mm × 11.43 mm
Pixels resolution	640 × 480	640 × 480
Field of view	50° × 38.55°	13.30° × 10.05° (at center)
Angular resolution	4.69 arc min ~12.5 pixels/deg	1.25 arc min ~48 pixels/deg

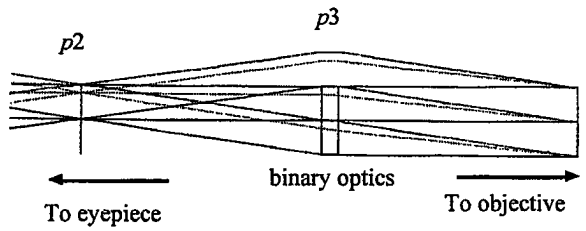

Total track 59.22 mm

Fig. 6. Duplicator layout with binary optics.

The number of phase levels must be sufficiently large for the fabricated lens to yield high efficiency. The f-number of the duplicator is calculated to be 3.6. When four levels ($m = 4$) are assumed, the minimum feature size p is 1 μm for a wavelength of 550 nm. An element with this feature size can be easily fabricated. In this case, an element with one binary optics surface can be designed. However, the theoretical efficiency of the lens at its edges is limited to 81%.[32] Note that potential edge effects for either binary optical arrays or elements are automatically accounted for in the computation of the modulation transfer function (MTF) by the optical design software, given that apertures are set correctly.

To have higher efficiency at the expense of an increase in the cost of fabrication, one can adopt more phase levels. For eight levels, p becomes half a micrometer. The efficiency then increases to 95%. Note that a feature size of half a micrometer may be difficult to achieve in some facility, but it is commonly achieved with state-of-the-art technology. If it is the case, however, the power of this element can be distributed in more than one surface. When two surfaces with 95% efficiency are used, the efficiency of the element is kept at 90%. The design given in Fig. 6 shows two silica binary optic surfaces located in the plane p_3, and the minimum feature size is set to 1 μm in this case. Figures 7 and 8 show the rayfan and the MTF plots of the binary optics duplicator, respectively. The required spatial frequency at the duplicator is 37 line pairs/mm. (320/8.635 = 37.1 line pairs/mm, where 320 is the largest number of

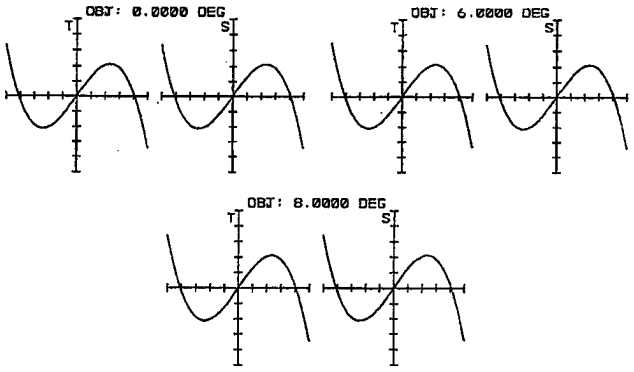

Maximum scale: 20 μm

Fig. 7. Duplicator rayfan.

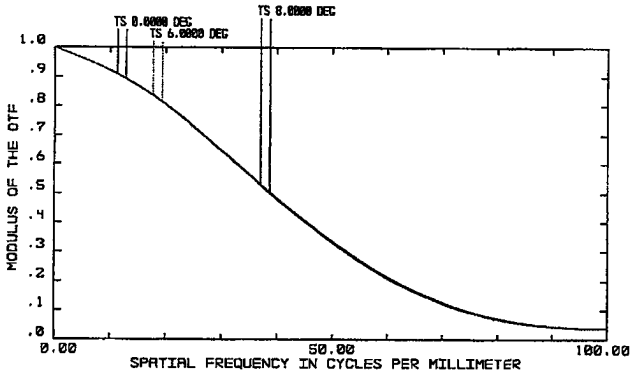

Fig. 8. Duplicator MTF.

line pairs in the display (640 × 380), and a_2 equals 8.635 mm as shown in Table 2.)

An efficiency of less than 100% results in scattered light in the optical system that causes reduction in the MTF from its designed nominal value. Frequently, a 90% efficiency yields 10% of scattered light. The effect on the MTF is an overall decrease of the MTF curve by a constant amount. In our example, the value of the decrease in MTF can be estimated when the value of the MTF at a low frequency of 1 or 2 cycles/mm is multiplied by 10%. Let us consider the MTF at position 0 on the axis shown in Fig. 11. This is the lowest plain curve for position zero. At 2 cycles/mm, the MTF value is 0.975. A 10% decrease corresponds to a reduction of approximately 0.1 in the MTF that must be subtracted from the values of the MTF across the spectrum. A plot of the estimated effective value of the MTF to account for 10% scatter is shown in Fig. 11 as the lowest dash curve. The effect of scatter for a HMD is minimal, and our experience with designing and building such systems has revealed that it is negligible. This would not be the case of night-vision HMD's in which light is scarce and scatter can significantly degrade the performance of such systems.

When considering Fig. 6, note that the duplicator solution presented in Fig. 4(b) was selected over that presented in Fig. 4(a). The vignetting occurring at the duplicator was discussed in Section 4. We adopted this configuration, as it is the simplest configuration of the two. Moreover, it contributes to minimizing potential alignment problems that might occur when a lenslet array in the plane p_2 and a binary lenslet array (or a pair of them as discussed above) in the plane p_3 are simultaneously used. In the implementation presented here, a single binary optics element was adopted for the duplicator to demonstrate the entire design in its simplest form at the expense of vignetting. With increase in cost, an additional lenslet array may be added in the plane p_2 to reduce vignetting if maximizing light output is an important design criterion.

One of the potential downfalls of using binary optics in any optical system is the degradation of image quality, which is a result of incorrectly handling substantial chromatic aberrations. Because binary optics has the opposite chromatic aberrations as

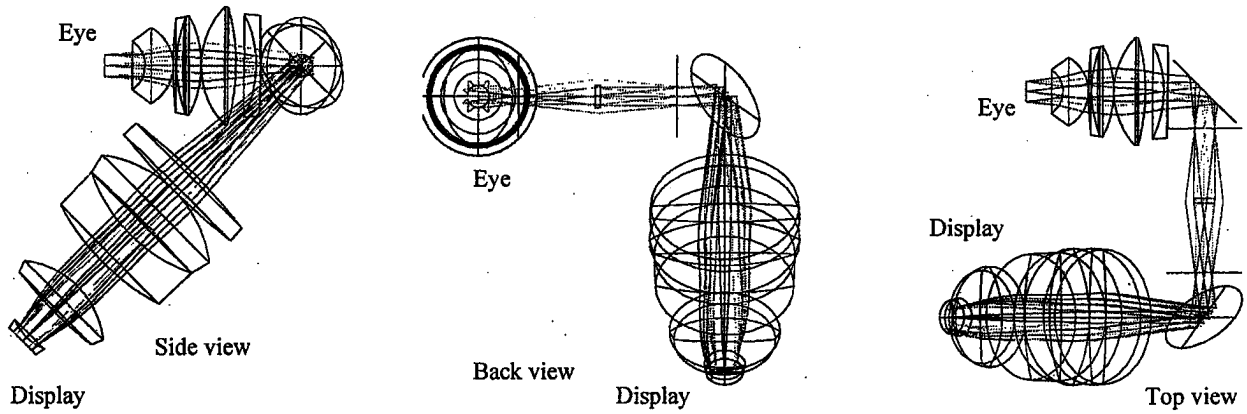

Fig. 9. Possible design and geometric configuration of the OHRI HMD.

refractive optics, it is most commonly used in combination with conventional optics for imaging systems. Moreover, imaging power may be distributed among diffractive and refractive elements to balance aberrations; although this is possible, it is not usually done. In a first effort to demonstrate the conceptual design of this new approach to inset displays, we assume monochromatic light and employ only diffractive elements at the duplicator for simplicity. For multispectrum light, some refractive elements might be required in the duplicator design, and variations in diffraction efficiencies over the spectrum will need to be accounted for in the design and the performance assessment. A complete assessment of the use of diffractive elements for a color display is beyond the scope of this paper.

7. Design and Overall Performance of the Optoelectronic High-Resolution Inset Head-Mounted Display

A design configuration of the entire system is shown in Fig. 9. The system is folded at several places to keep the center of gravity low and close to the head. Figures 10 and 11 show the performance of the entire system at several duplicator positions, indexed from 0 to 8 according to Fig. 5. These figures show that the system is capable of resolving spatial frequencies above the required level of 21 line pair/mm (320/15.240 = 21.0 line pair/mm, where 320 is the largest number of line pairs in the display (640 × 380), and a_5 equals 15.240 mm as shown in Table 2) (MTF > 20%) except at the largest field angle (MTF > 10%). Although the system demonstrated here was obtained after optimization of each optical component (i.e., objective, duplicator, and eyepiece) independently, the performance of the system may be improved by optimizing all components simultaneously.

8. Proposed Eye-Tracker System for the Optoelectronic High-Resolution Inset Head-Mounted Display

The OHRI HMD system requires that the relative orientation of the eyes be known. Therefore an understanding of eye movement might appear critical. Although the primary eye movements are saccadic, smooth-pursuit, and vergence and the fastest motions are that of saccades (initiated approximately 200 ms after the target object leaves the fovea[34] at speeds of as much as 900 deg/s), the parameter of interest for an inset HMD is the duration of a fixation for which the inset will be positioned. The speed of smooth-pursuit movements is typically slower, reaching 100 deg/s.[34] Other types of eye movements, including the vestibular-ocular reflex, optokinetic response, and nystagmus combine aspects of the saccadic and the smooth-pursuit movements.

It is widely accepted in the vision literature that it takes typically 100 ms to process new visual information (numbers from 80 to 150 ms are argued among visual scientists). As a result, a fixation is typically defined as a 100-ms pause in eye movement.[35] It is known that microsaccades of average amplitude 30 arc min do occur during fixation, but unless the deviation is greater than 2.5°, we shall consider that it is one single fixation for our application. For high-resolution inset HMD's, the time required for a fixation to occur (i.e., 100 ms) or, more conservatively, the time required for the average number of fixations per second (i.e., 4 fixations/s) determines the required bandwidth of the eye tracker. Therefore a 10-Hz bandwidth is required based on the time of a fixation, or a 4-Hz bandwidth is required based on the average number of fixations per second. With a display device updating information at 72 frames/s, we shall be limited in most tracking schemes by the tracking device and not by the display frame rate. Note, however, that current frame rates of tracking devices are largely sufficient to monitor changes in fixations. Furthermore, the range of saccadic and smooth-pursuit eye movements without head motion is 1–30° relative to the current eye position,[29] requiring our eye tracker to measure as high as 30° displacements accurately.

As a result of these observations, an eye tracker based on the principle of electro-oculography (EOG) satisfies our requirements. EOG is a method of recording voltage changes due to eye rotation.[19] In the eye, a potential difference of as much as 1.0 mV exists

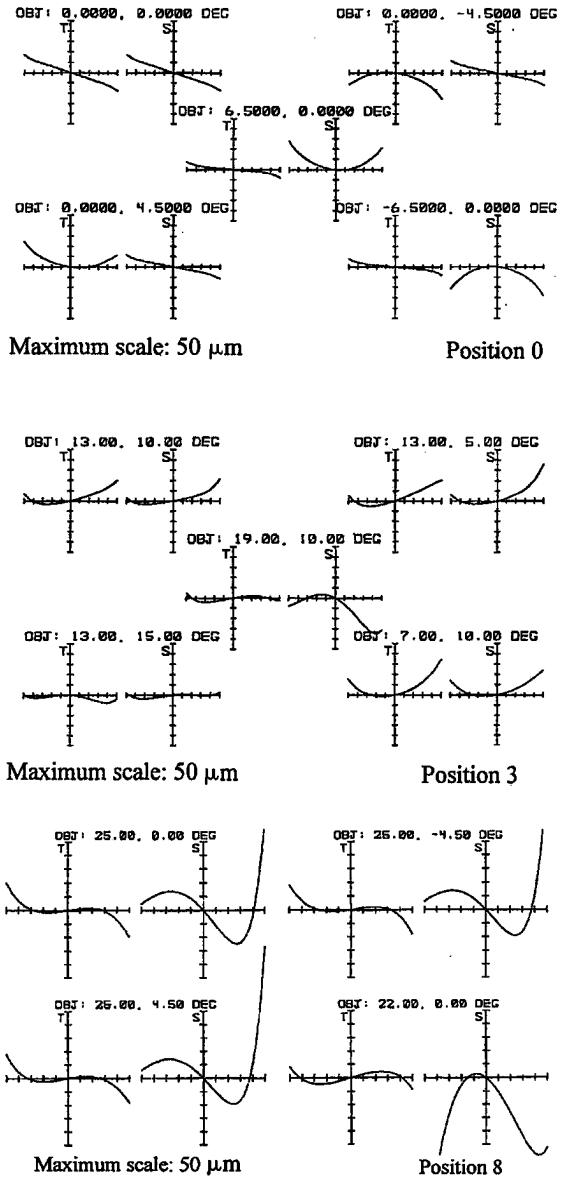

Fig. 10. (a) Entire system rayfan at several inset positions.

between the cornea and the retina, with the cornea being positive with respect to the retina.[29] When the eye moves, this corneo-retinal potential (CRP) causes a change in potential in the area immediately surrounding the eye. By measuring this change in potential at certain locations around the eye, one can determine eye position indirectly. With proper electrode placement, which is detailed hereafter, a tracking accuracy of ± 1 degrees is achievable,[19] with a range of $\pm 70°$.[29] In addition, a frequency response of as much as 15 Hz is achievable with EOG. (Note that infrared eye trackers, with rates from 60 to 240 Hz, can also be implemented.[35]) Finally, the recording electronics used for EOG can be miniaturized to decrease overall weight and system size.

The design of the eye tracker involves minimizing electrical interference while providing adequate output response. Electromuscular signals, galvanic skin response (GSR), and electroencephalography (EEG) signals can cause interference when measuring the CRP.[36] To lessen the effects of electromuscular signals (caused by facial movements), Ag–AgCl electrodes are placed as close to the orbital bone boundary as possible. Placing the electrodes close to the eye also increases the amplitude of the CRP signal. However, the CRP is still small and amplification of the signal is necessary. Additionally, the presence of EEG signals at the electrodes prevents linear amplification. To minimize EEG interference, a differential amplifier configuration with a high common-mode rejection ratio is used.[36] Removing oils from the perspective electrode location can minimize GSR. Still, measuring the CRP from the same locations each time better reduces the effects of GSR by providing a repeatable resistance. Because the CRP may change as a factor of lighting and metabolic rate, a quick calibration must be performed for each use of the system.

EOG eye-tracking technology is attractive for the OHRI HMD because it is positioned around the eyes

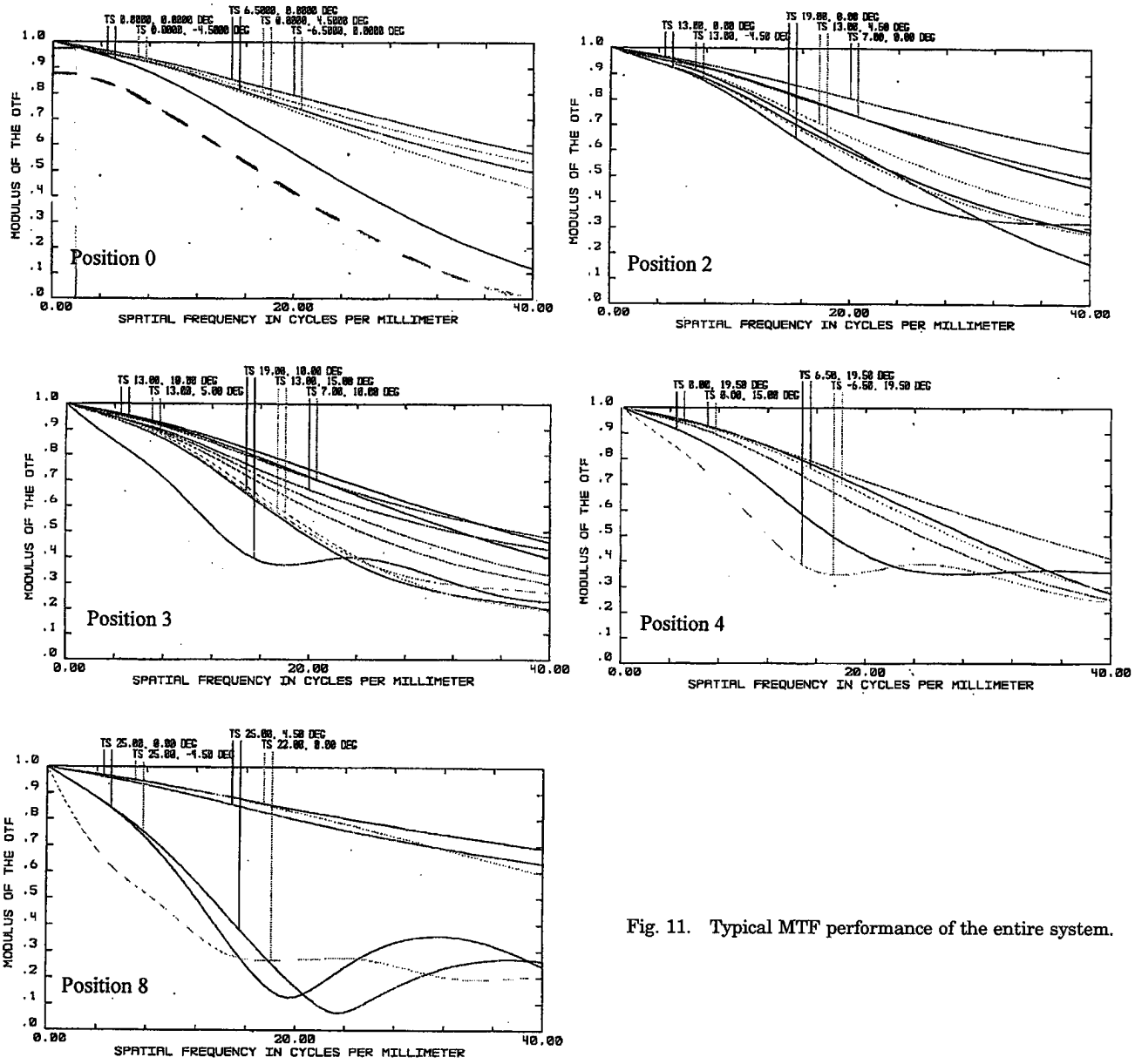

Fig. 11. Typical MTF performance of the entire system.

and therefore is nonobtrusive. In addition, it requires no exhaustive user preparation and can be integrated easily with our prototype. Finally, the wide availability of the electronics required, the capability of miniaturization, and the low cost of such devices suggest that the use of EOG in HMD's will become commonplace.

9. Practical Limitations

Although the proposed approach may achieve our goal as a prototype, it has several practical limitations. These issues are first discussed and alternative approaches as well as their respective advantages and limitations are described.

One of the difficulties is to keep the duplicated images free of both distortion and field curvature. When there is distortion, the gaps between the duplicated images become highly visible and it becomes impossible to form an inset image with four neighboring duplicate images as described earlier. The visual quality is unevenly degraded by field curvature as well. Furthermore, the alignment issue also becomes critical for the objective and the duplicator systems that must generate duplicated images from a single inset image. Finally, once constructed, the entire system must be packaged in a light and rigid helmet system to guarantee the portability and the durability of the system. Diffraction efficiency at the duplicator, as discussed in Section 6, and reflection at multiple surfaces decrease the MTF ratios. We estimate that decreases of less than 15% overall can be achieved with current technologies. Antireflection coatings can be effectively used to reduce reflection at lens surfaces, for example, and more levels in diffractive optical elements can be utilized to yield higher efficiencies at the expense of increase in fabrication cost.

Recent advances in producing miniature active matrix displays and their prospected wide use in various fields seems to indicate that using multiple displays, instead of optically duplicated ones, may be advantageous. This approach eliminates the alignment problem and decreases the volume and the weight of the system. This approach differs from other multiple displays system because the entire view is rendered by a single background display and only the inset is rendered by one of the inset displays at a time. The benefit of separating two sources, namely, the background and the inset, is maintained. Furthermore, the inset size can be enlarged by software within the bandwidth limit. However, the problem of completely eliminating the gaps between the inset displays remains a challenge. For the miniature displays in consideration, the gaps are relatively large (stretching approximately 20% of the displayable area in each direction), leading to a nonviable or at least a highly suboptimal approach. However, since the eye position and the visual angle are limited, if a display with a very small peripheral area was made available, one can minimize these peripheral gaps by using an array of lenses with each lens directly attached to each display.

Another problem with the proposed design is the merging of two sources. The current eyepiece that must allocate a large space between the eyepiece lens and its focal plane introduces a scalability problem for field of view. This space was necessary for merging the two optical paths. This construction is not necessary if a transparent display is used for the background as well as the insets. In this case, both the background and the multiple inset displays can be illuminated from behind. However, the problem of positioning two surfaces, the background and the insets, on a single plane is not possible and a lack in exact superimposition yields parallax errors with various eye locations behind the HMD. Given the physical dimensions of such displays, an analysis of the magnitude of such errors needs to be conducted if such a scheme is to be considered.

10. Conclusion

The approach to the design of a novel high-resolution inset HMD referred to as the OHRI HMD was presented. The principle of insertion for the high-resolution inset, which involved no mechanical components but rather solely optoelectronic devices, was shown. The apparent benefit of the OHRI HMD is its potential for providing a relatively large field of view (i.e., 630) as well as a high-resolution image (i.e., 1.25 arc min for inset and 4.7 arc min for background) in addition to being portable. Moreover, such a system also supports various gaze-point-oriented interaction methods unlike systems with no eye-tracking capability.

The authors thank Reinhardt Männer and Steffen Noehte at the University of Mannheim for their interesting discussions and equipment support, Hudson Welch at Digital Optics Corporation for his assistance with binary optics specification and fabrication, Applied Science Laboratories for their assistance with eye-tracker requirements, and Robert Kennedy from RSK Assessments, Inc. for pointing us to the literature in saccadic suppressions and the literature on electro-oculography. This research was supported in part by the Office of Naval Research, grant N000149710654 and the National Library of Medicine under grant 1-R29-LM06322-01A1.

References

1. S. S. Fisher, "Virtual interface environments," in *The Art of Human-Computer Interface Design*, B. Laurel ed. (Addison-Wesley, Menlo Park, Calif., 1990), 423–438.
2. D. Foley, "Interfaces for Advanced Computing," Sci. Am. **257**(4), 126–135 (1987).
3. J. C. Chung, M. R. Harris, F. P. Brooks, H. Fuchs, M. T. Kelley, J. Hughes, M. Ouh-Young, C. Cheung, R. L. Holloway, and M. Pique, "Exploring virtual worlds with head-mounted displays," in *Three-Dimensional Visualization and Display Technologies*, S. S. Fisher and W. E. Robbins, eds., Proc. SPIE **1083,** 42–52 (1989).
4. G. Burdea and P. Coiffet, *Virtual Reality Technology* (Wiley, New York, 1994).
5. R. E. Cole, C. Ikehara, and J. O. Merritt, "A low cost helmet-mounted camera/display system for field testing teleoperator tasks," in *Stereoscopic Displays and Applications III*, J. O. Merritt and S. S. Fisher, eds., Proc. SPIE **1669,** 228–235 (1992).
6. S. S. Fisher, M. McGreevy, J. Humphries, and W. Robinett, "Virtual environment display system," presented at the Association for Computing Machinery Workshop on Interactive 3D Graphics, Chapel Hill, North Carolina, 23–24 Oct. 1986.
7. S. S. Fisher, M. W. McGreevy, J. Humphries, and W. Robinett, "Virtual interface environment for telepresence applications," in *Proceedings of the American Nuclear Society International Topical Meeting on Remote Systems and Robotics in Hostile Environments*, J. D. Berger, ed. (American Nuclear Society, Lagrange Park, Ill., 1987).
8. C. Herot, "Spatial management of data," ACM Trans. Database Systems **5**(4), 493–514 (1980).
9. D. Thalmann, "Using virtual reality techniques in the animation process," in *Virtual Reality Systems*, R. A. Earnshaw, M. A. Gigante, and H. Jones, eds. (Academic, Reading, Mass., 1993).
10. E. M. Howlett, "High-resolution inserts in wide-angle head-mounted stereoscopic displays," in *Stereoscopic Displays and Applications III*, J. O. Merritt and S. S. Fisher, eds., Proc. SPIE **1669,** 193–203 (1992).
11. H. Davson, *Physiology of the Eye*, 5th ed. (Pergamon, New York, 1990).
12. R. A. Moses, *Adlers Physiology of the Eye* (Mosby, St. Louis, Mo., 1970).
13. G. Westheimer, "The eye as an optical instrument," in *Handbook of Perception and Human Performance* 1(4) (Wiley-Interscience, New York, 1986), Vol. 1, Chap. 4.
14. F. J. Ferrin, "Survey of helmet tracking technologies," in *Large Screen Projection, Avionic, and Helmet-Mounted Displays*, H. M. Assenheim, R. A. Flasck, T. M. Lippert, J. Bentz, and W. Groves, eds., Proc. SPIE **1456,** 86–94 (1991).
15. R. A. Bolt, "Gaze-orchestrated dynamic windows," Comput. Graphics, **15**(3), 109–119 (1981).
16. S. Bryson, "Interaction of objects in a virtual environment: a two-point paradigm," in *Stereoscopic Displays and Application II*, J. O. Merritt and S. S. Fisher, eds., Proc. SPIE **1457,** 180–187 (1991).

17. H. Jacoby and S. R. Ellis, "Using virtual menus in a virtual environment," Proc. SPIE **1668,** 39–47 (1992).
18. T. P. Colgate, "Reaction and response time of individuals reacting to auditory, visual, and tactile stimuli," Research Quarterly **39,** 783–784 (1968).
19. P. J. Oster and J. A. Stern, "Measurement of Eye Movement," in *Techniques of Psychophysiology*, I. Martin, and P. H. Venables, eds. (Wiley, New York, 1980).
20. H. Girolamo, "Notional helmet concepts: a survey of near-term and future technologies," U.S. Army NATICK Technical Report NATIK/TR-91/017 (U.S. Army, 1991).
21. R. Dodge, "Five types of eye movement in the horizontal meridian plane of the field of regard," Am. J. Phys. **8,** 307–329 (1903).
22. F. Volkman, L. A. Riggs, K. D. White, and R. K. Moore, "Contrast sensitivity during saccadic eye movements," Vis. Res. **18,** 1193–1199 (1978).
23. F. Volkman "Human visual suppression," Vis. Res. **26,** 1401–1416 (1986).
24. R. Burbidge and P. M. Murray, "Hardware improvement to the helmet-mounted projector on the visual display research tool at the Naval Training Systems Center," in *Helmet-Mounted Displays*, J. T. Carollo, ed., Proc. SPIE **1116,** 52–60 (1989).
25. M. L. Thomas, W. P. Siegmund, S. E. Antos, and R. M. Robinson, "Fiber optic development for use on the fiber optic helmet-mounted display," in *Helmet-Mounted Displays*, J. T. Carollo, ed., Proc. SPIE **1116,** 90–101 (1989).
26. A. Yoshida, J. P. Rolland, and J. H. Reif, "Design and applications of a high-resolution insert head-mounted-display," *Proceedings of the IEEE Virtual Reality Annual International Symposium* (Institute of Electrical and Electronics Engineers, New York, 1995), 84–93.
27. A. Yoshida, J. P. Rolland, and J. H. Reif, "Optical design and analysis of a head-mounted display with a high-resolution insert," in *Novel Optical Systems Design and Optimization*, J. M. Sasian, ed., Proc. SPIE **2537,** 71–82 (1995).
28. Applied Science Laboratories, *Eye Tracking Systems Handbook* (Applied Science Laboratories, Waltham, Mass., 1992).
29. L. Young and D. Sheena, "Survey of eye movement recording methods," Behav. Res. Methods Instrum. Comput. **7,** 397–429 (1975).
30. G. Sharp, Boulder Nonlinear Systems, Inc., 1898 South Flatiron Court, Boulder, Colo. 80301 (personal communication, 1997).
31. P. K. Doenges, Evans and Sutherland, 600 Komas Drive, P.O. Box 58700, Salt Lake City, Utah 84158 (personal communication, 1997).
32. J. P. Salerno, "Single crystal silicon AMLCDs," presented at the International Workshop on Active Matrix Liquid Crystal Displays, 14th International Display Research Conference, Monterey, Calif., 1–7 September 1994.
33. J. Jahns, "Diffractive optical elements for optical computers," in *Optical Computing Hardware*, J. Jahns and S. H. Lee, ed. (Academic, Boston, Mass., 1994).
34. M. E. Goldberg, H. M. Eggers, and P. Gouras, "The Ocular Motor System," in *Principles of Neural Science*, 3rd ed, E. R. Kandel, J. H. Schwartz, and T. M. Jessell, ed. (Appleton & Lange, Norwalk, Conn., 1991).
35. J. Borah, Applied Science Laboratories, 175 Middlesex Turnpike, Bedford, Mass. 01730-1428 (personal communication, 1997).
36. M. A. Wiedl, "Some Practical Consideration in Eye Movement Recording Methodologies" (Pacific Missile Test Center, Point Mugu, Calif., 1977).